J. Phys. B: At. Mol. Opt. Phys. **32** (1999) L139–L144. Printed in the UK PII: S0953-4075(99)00702-6

LETTER TO THE EDITOR

Electron detachment in H^+–H^- collisions

F Melchert, S Krüdener, K Huber and E Salzborn
Institut für Kernphysik, Justus-Liebig-Universität Giessen, D-35392 Giessen, Germany

Received 5 January 1999, in final form 5 February 1999

Abstract. Using the crossed-beams technique, we have measured absolute cross sections for the total production of H^0 in collisions between H^+ and H^- ions

$$H_a^+ + H_b^- \rightarrow H_b^0 + \cdots$$

by means of a beam-pulsing method for the H^0 detection for centre-of-mass energies between 1.4 and 39.8 keV. From the measured data cross sections for the electron detachment process

$$H_a^+ + H_b^- \rightarrow H_a^+ + H_b^0 + e^-$$

were calculated using the total cross sections for mutual neutralization measured previously. The electron detachment results are in very good agreement with recent theoretical calculations.

Electron detachment in collisions between positive and negative hydrogen ions

$$H_a^+ + H_b^- \rightarrow H_a^+ + H_b^0 + e^- \tag{1}$$

is one of the fundamental reactions in few-electron collision systems. The negative hydrogen ion H^- plays a role in three-body Coulombic systems that is comparable to the central place of the hydrogen atom H^0 in two-body quantum mechanics. Several reaction channels in $H^+ + H^-$ collisions have been studied extensively, e.g. mutual neutralization $H_a^+ + H_b^- \rightarrow H_a^0 + H_b^0$, both by experiment, e.g. [1–6], and by theory [7–9]. At low collision energies, the split-shell ($1s1s'$) single-configuration description of the H^- ion was often invoked. According to this picture, one of the two H^- electrons lies in an almost hydrogenic 1s orbital, whereas the second loosely bound $1s'$ electron occupies a diffuse orbital whose radius is about 4 a_0. In mutual neutralization collisions with H^+, the additional electron is captured, while the atomic core remains mainly undisturbed. At high collision energies, this treatment was found to be no longer valid [8] and capture of the core electron had to be taken into account.

Here we report measurements of absolute cross sections σ_T for the total production of hydrogen atoms

$$H_a^+ + H_b^- \rightarrow H_b^0 + \cdots. \tag{2}$$

The H_b^0 atoms can be produced either by electron detachment (1) with a cross section σ_D, or by mutual neutralization

$$H_a^+ + H_b^- \rightarrow H_a^0 + H_b^0 \tag{3}$$

with a cross section σ_M. Obviously, the lost electron can be either ejected or captured: $\sigma_D + \sigma_M = \sigma_T$. The mutual neutralization cross section σ_M measured earlier by Schön *et al* [5] allows us to calculate the electron detachment cross section σ_D from the measured cross section σ_T by the relation $\sigma_D = \sigma_T - \sigma_M$. In figure 1, measured and calculated cross sections, σ_T, σ_M and σ_D are plotted as a function of the centre-of-mass (CM) collision energy E_{CM}. At

0953-4075/99/060139+06$19.50

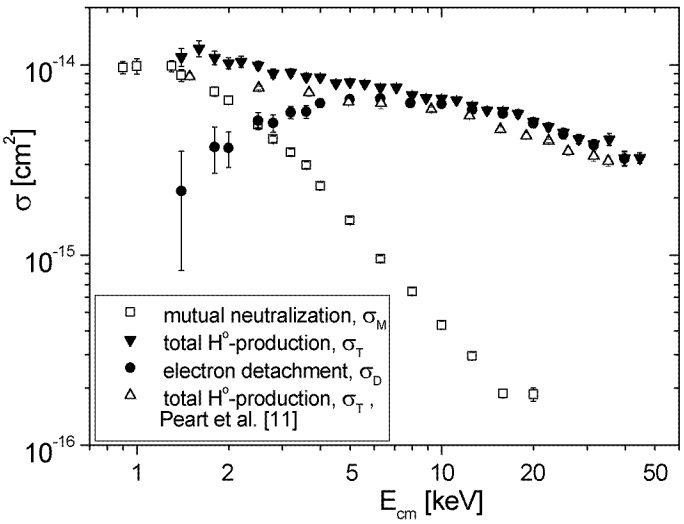

Figure 1. Cross sections for reactions (1)–(3) in $H^+ + H^-$ collisions. σ_T was measured, σ_M was taken from earlier work [5] and σ_D was calculated from $\sigma_D = \sigma_T - \sigma_M$. For comparison, earlier measurements of σ_T by Peart *et al* [11] are included.

low collision energies, the detachment cross section σ_D has a large statistical error due to the subtraction of σ_M from σ_T which are of almost equal magnitude.

The crossed-beams technique employed to investigate the electron detachment was described in full detail previously [10]. In short, the experimental arrangement consists of an ultra-high vacuum (UHV) chamber, a 'slow' beamline $\mathcal{A}$ and a 'fast' beamline $\mathcal{B}$. After momentum analysis, both ion beams are collimated by adjustable four-jaw slits to approximately 1.5 mm $\times$ 1.5 mm before they enter the UHV chamber. Shortly before intersection at an angle $\alpha = 45^\circ$, both ion beams are cleaned by electrostatic deflectors from particles in other charge states resulting from charge-changing collisions in the residual gas.

In beamline $\mathcal{A}$, H_a^+ ions are produced by a 5 GHz electron cyclotron resonance (ECR) ion source, analysed, focused and fed into the UHV interaction chamber. The parent ion beam is measured in a Faraday cup, and ions which have changed their charge either in ion–ion collisions or by interactions with the residual gas are not detected. In beamline $\mathcal{B}$, negative H_b^- ions are produced by a radio-frequency (RF) ion source mounted on a high-voltage terminal. After acceleration, analysis and focusing the beam is bent by an electrostatic deflector towards the interaction volume. After the interaction, H_b^0 atoms are separated by a second electrostatic deflector from the H_b^- parent ion beam and detected in a channeltron-based single-particle detector.

Although the crossed-beams technique, in principle, appears to be straightforward, inherent difficulties arise from the small target thickness provided by the ion beams. Even at ultra-high vacuum conditions ($<10^{-10}$ mbar) in the interaction region the residual gas density exceeds the ion densities within the beams. These conditions result in a comparatively low signal count rate (typically $\sim$100 cps) and a poor signal-to-noise ratio (typically 10^{-2}).

The electron detachment reaction (1) leaves the H_a^+ collision partner in its initial charge state. Therefore, a coincident detection of the heavy reaction products is not possible. A beam-modulation technique [10] was used instead in order to distinguish between signal and background events. Basically, the actual time spectrum of H_b^0 atoms is recorded in beamline $\mathcal{B}$,

while both ion beams are chopped by fast electrostatic deflection. Each pulse cycle of 2.46 ms length, which is repeated at 407 Hz, is subdivided by clock pulses into 256 time channels. Furthermore, each pulse cycle consists of four sections. In section I, both beams are switched off and the H_b^0 detector records only background events of a rate N_I which are not caused by the ion beams. In section II, beamline $\mathcal{A}$ is switched on which is not analysed, but generates some background events at a rate of N_{II} in the H_b^0 detector in beamline $\mathcal{B}$. In section III, beamline $\mathcal{A}$ is switched off and beamline $\mathcal{B}$ is switched on. In this section, background events by electron detachment in the residual gas are registered in the H_b^0 detector at a count rate of N_{III}. Finally, in section IV both ion beams are switched on and the ion–ion signal rate R is detected on top of the different background contributions. From $R = (N_I + N_{IV}) - (N_{II} + N_{III})$ the signal rate can be determined. Usually, R is small compared with N_i, and large numbers have to be subtracted from each other to yield R. Therefore the count rates N_i have to be measured very carefully. Detector deadtime corrections which are usually less than 1% can reach the magnitude of the signal rate R. We carefully checked them systematically by introducing a programmable computer-controlled deadtime which exceeded the actual detector deadtime. Measurements have been made for various programmed deadtimes, and the apparent cross sections did depend on the programmed deadtime, while the deadtime-corrected cross sections did not. The performance of the apparatus can be judged from typical experimental parameters of cross section measurements listed in table 1 for three centre-of-mass energies.

Table 1. Typical experimental parameters of cross section measurements σ_T for the reaction $H_a^+ + H_b^- \rightarrow H_b^0 + \cdots$ at CM energies $E_{CM} = 3.55$, 10.0 and 39.9 keV. E_{H^+}, E_{H^-}, I_{H^+} and I_{H^-} denote the respective laboratory energies and currents of the H^+ and the H^- ion beams, N_{H^0} the detector count rate of the H^0 reaction products in beam line $\mathcal{B}$. R, true ion–ion signal rate; t, actual measurement time.

E_{CM} (keV)	E_{H^+} (keV)	E_{H^-} (keV)	I_{H^+} (nA)	I_{H^-} (nA)	N_{H^0} (s^{-1})	R (s^{-1})	t (s)
3.55	10.0	13.6	796	14.9	6600	125	500
10.0	17.0	39.7	3011	11.5	7800	169	500
39.9	10.0	118	950	15.0	2400	60.1	500

Since the average orbital radius is about 4 au for the additional 1s′ electron within the H^- ion, large impact parameters contribute to the electron detachment process. Therefore, angular scattering in beamline $\mathcal{B}$ is expected to be of minor importance. This was verified experimentally by 'flat-topped-peak' measurements in which the measured cross sections were found to be independent of the analyser voltages over a reasonable range.

Our measured cross sections are listed in table 2 with 90% confidence limits of random error. All cross sections are subject to an estimated additional uncertainty of $\pm 15\%$, resulting mainly from the error associated with the detection efficiency of the single-particle detector and the detector deadtime corrections.

Electron detachment (1) was first investigated experimentally by Peart *et al* [11] as early as 1976. They measured cross sections σ_T for the total production of hydrogen atoms (2) and had to subtract cross sections σ_M for mutual neutralization (3). In 1976, no cross sections σ_M were measured in the relevant energy range, and Peart *et al* had to extrapolate measured [1, 2] low-energy data σ_M to higher collision energies. In 1987, Schön *et al* [5] showed that this extrapolation resulted in a significant overestimation of σ_M and, as a consequence, led to an underestimation of the electron detachment cross section $\sigma_D = \sigma_T - \sigma_M$. Our cross sections σ_D exceed Peart's data by a factor of two at $E_{CM} = 2.5$ keV. For higher energies, this factor

Table 2. Measured cross sections σ_T for the production of hydrogen atoms $H_a^+ + H_b^- \rightarrow H_b^0 + \cdots$. The uncertainties of the measured data represent the 90% confidence limits of statistical error only. For completeness, cross sections σ_M for mutual neutralization (3) published earlier [5] are included. Cross sections σ_D for electron detachment (1) are calculated using $\sigma_D = \sigma_T - \sigma_M$.

E_{CM} (keV)	Measured cross section σ_T (10^{-16} cm^2)	Measured cross section σ_M (10^{-15} cm^2)	Calculated cross section σ_D (10^{-15} cm^2)
1.4	88.0 ± 6.4	11.0 ± 1.2	2.17 ± 1.34
1.8	72.3 ± 4.0	10.9 ± 0.9	3.70 ± 1.01
2.0	65.1 ± 3.1	10.2 ± 0.7	3.66 ± 0.78
2.5	48.5 ± 1.9	9.93 ± 0.48	5.08 ± 0.52
2.8	40.6 ± 1.6	9.01 ± 0.50	4.94 ± 0.52
3.2	34.7 ± 1.4	9.09 ± 0.40	5.62 ± 0.42
3.6	29.7 ± 1.2	8.63 ± 0.41	5.66 ± 0.43
4.0	23.1 ± 1.0	8.59 ± 0.32	6.28 ± 0.33
5.0	15.2 ± 0.6	8.11 ± 0.27	6.59 ± 0.28
6.3	9.54 ± 0.39	7.60 ± 0.27	6.65 ± 0.27
8.0	6.43 ± 0.28	6.93 ± 0.22	6.29 ± 0.22
10.0	4.28 ± 0.21	6.65 ± 0.23	6.22 ± 0.23
12.6	2.94 ± 0.14	6.10 ± 0.23	5.81 ± 0.23
15.9	1.87 ± 0.10	5.73 ± 0.22	5.54 ± 0.22
20.0	1.85 ± 0.152	5.02 ± 0.25	4.92 ± 0.25
25.1	0.874 ± 0.185	4.40 ± 0.24	4.31 ± 0.24
31.6	0.399 ± 0.059	3.83 ± 0.21	3.79 ± 0.21
39.8	0.189 ± 0.019	3.23 ± 0.28	3.21 ± 0.28

decreases to about 1.3 at $E_{CM} = 35$ keV. This discrepancy can be partly resolved using the cross sections σ_M measured by Schön *et al*. A direct comparison of our measured σ_T data with the results of Peart *et al* [11] is depicted in figure 1. The experimental results of σ_D are compared to different theories in figure 2.

In 1983, Sidis *et al* [7] investigated the ionic–covalent problem in the $H^+ + H^-$ collision system theoretically and calculated cross sections for (1) within a quasimolecular approach, including electron translational factors for low collision energies $E_{CM} < 10$ keV. Their results confirmed the experimental data by Peart *et al*. One year later, Fussen and Claeys [12] performed a two-state model calculation for electron detachment (1) in which both states are coupled by the asymptotic part of the long-range dipole interaction. In the energy range $E_{CM} < 10$ keV they also confirmed Peart's measurements, but they extended their calculation to higher energies where Peart's results were overestimated.

In 1988, Ermolaev [8] carried out close-coupling calculations within the semiclassical impact parameter approximation, with the wavefunction expanded in terms of a two-centre basis of travelling atomic orbitals with up to 51 states. For low energies ($E_{CM} < 5$ keV), the main contribution to the electron detachment (1) channel is obtained using a one-active-electron model, while for higher energies Ermolaev employed a modified version of an independent particle model, where either the 'inner' or 'outer' electron can be detached. However, Ermolaev found the contribution of the 'inner' electron for electron detachment (1) to be less important than for mutual neutralization (3).

Ermolaev's basis AO-29 consisting of 29 atomic states overestimated Peart's experiment at low collision energies $E_{CM} < 3$ keV, but is in good agreement with our present results. As E_{CM} increases, the representation of the continuum states by AO-29 becomes less adequate. Extension of the basis size to 36 states (AO-36) increases the calculated cross section, but for

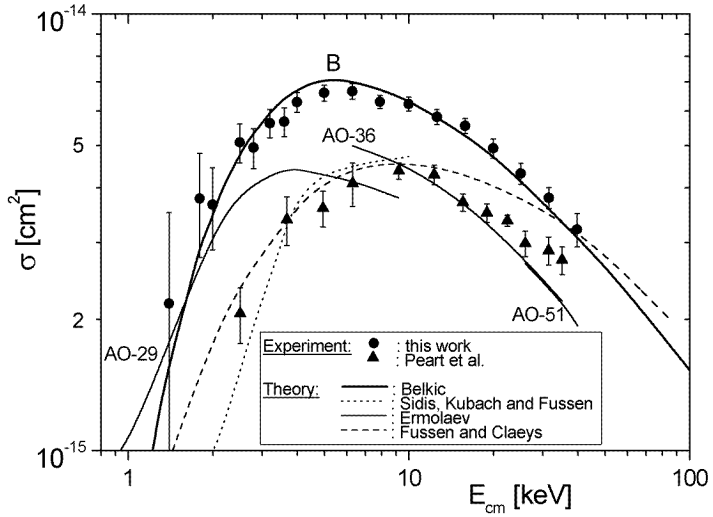

Figure 2. Cross section σ_D for the electron detachment reaction $H_a^+ + H_b^- \rightarrow H_a^+ + H_b^0 + e^-$ as a function of the CM collision energy. The present data (●) and previous data (▲ [11]) are compared with recent theoretical results by Belkić [13] and earlier work by Sidis *et al* [7], Ermolaev [8] and Fussen and Claeys [12]. The three curves by Ermolaev were obtained with three different atomic-orbital basis sets AO-29, AO-36 and AO-51 as indicated in the figure.

low E_{CM}, this expansion is less accurate than AO-29 because it does not include projectile states with the principal quantum number $n > 2$. At high $E_{CM} > 25$ keV, the AO-36 results coincide with the even larger AO-51 basis indicating that no finite-basis effect is important in Ermolaev's calculation. Compared to our experimental results, Ermolaev's AO-36 and AO-51 results underestimate the electron detachment cross section by almost a factor of two, while agreement was found with AO-29 at low collision energies.

Very recently, Belkić [13] investigated the electron detachment process (1) using the four-body correlated distorted-wave formalism of scattering theory. He emphasized the combined role played by the long-range Coulomb distortion effects both on the incident plane wave and on the associated perturbation potentials. The eikonal Coulomb–Born model differs from the usual plane-wave Born method by inclusion of the long-range Coulombic effects between the active electron and the projectile in both the entrance and exit channels. However, in the 'prior' probability amplitude, the Coulomb interaction between the incident proton and the electron to be ejected is the only perturbation causing the transition. Belkić used another formalism, termed the modified Coulomb–Born model, introducing a new perturbation which includes three major additional potential operators [13]. As in the eikonal Coulomb–Born model, he ignored the interaction of the projectile with the 'inner' electron at all distances. Belkić's modified Coulomb–Born model exhibits the correct Bethe asymptote $\sigma_D \propto v^{-2} \ln v^2$ in the high-velocity limit.

In summary, we investigated electron detachment (1) in $H^+ + H^-$ collisions in the energy range 1.4 keV $< E_{CM} <$ 39.8 keV and found excellent agreement with recent calculations by Belkić [13] in the complete energy range.

This research was supported by BMFT under contract no 06-GI-333.

References

[1] Rundel R D, Aitken K L and Harrison M F A 1969 *J. Phys. B: At. Mol. Phys.* **2** 954–65
[2] Peart B, Grey R and Dolder K 1976 *J. Phys. B: At. Mol. Phys.* **9** L369–72
[3] Szücs S, Karemera M, Terao M and Brouillard F 1984 *J. Phys. B: At. Mol. Phys.* **17** 1613–22
[4] Peart B, Bennett M A and Dolder K 1985 *J. Phys. B: At. Mol. Phys.* **18** L439–44
[5] Schön W, Krüdener S, Melchert F, Rinn K, Wagner M and Salzborn E 1987 *J. Phys. B: At. Mol. Phys.* **20** L759–64
[6] Peart B and Hayton D A 1992 *J. Phys. B: At. Mol. Opt. Phys.* **25** 5109–19
[7] Sidis V, Kubach C and Fussen D 1983 *Phys. Rev.* A **27** 2431–46
[8] Ermolaev A M 1988 *J. Phys. B: At. Mol. Opt. Phys.* **21** 81–101
[9] Shingal R and Bransden B H 1990 *J. Phys. B: At. Mol. Opt. Phys.* **23** 1203–14
[10] Rinn K, Melchert F, Rink K and Salzborn E 1986 *J. Phys. B: At. Mol. Phys.* **19** 3717–26
[11] Peart B, Grey R and Dolder K T 1976 *J. Phys. B: At. Mol. Phys.* **9** 3047–53
[12] Fussen D and Claeys W 1984 *J. Phys. B: At. Mol. Phys.* **17** L89–93
[13] Belkić D 1997 *J. Phys. B: At. Mol. Opt. Phys.* **30** 1731–45